A Deep Learning-Based Methodology for Detecting and Visualizing Continuous Gravitational Waves

Emmanuel Pintelas(✉), Ioannis E. Livieris, and Panagiotis Pintelas

Department of Mathematics, University of Patras, Patras, Greece
{e.pintelas,livieris}@upatras.gr

Abstract. Since the Gravitational Waves' initial direct detection, a veil of mystery from the Universe has been lifted, ushering a new era of intriguing physics, as-tronomy, and astrophysics research. Unfortunately, since then, not much progress has been reported, because so far all of the detected Gravitational Waves fell only into the Binary bursting wave type (B-GWs), which are cre-ated via spinning binary compact objects such as black holes. Nowadays, as-tronomy scientists seek to detect a new type of gravitational waves called: Continuous Gravitational Waves (C-GWs). Unlike the complicated burst na-ture of B-GWs, C-GWs have elegant and much simpler form, being able to provide higher quality of information for the Universe exploration. Never-theless, C-GWs are much weaker comparing to the B-GWs, which makes them considerably harder to be detected. For this task, we propose a novel Deep-Learning-based methodology, being sensitive enough for detecting and visualizing C-GWs, based on Short-Time-Fourier data provided by LIGO. Based on extensive experimental simulations, our approach significantly outperformed the state-of-the-art approaches, for every applied experimental configuration, revealing the efficiency of the proposed methodology. Our expectation is that this work can potentially assist scientists to improve their detection sensitivity, leading to new Astrophysical discoveries, via the incor-poration of Data-Mining and Deep-Learning sciences.

Keywords: Deep learning · 2D image processing · SFT signal processing · remote sensing applications · ML methods for sensing systems

1 Introduction

Accelerated masses produce Gravitational Waves (GWs), which are disturbances or ripples in the curvature of spacetime that move as waves away from their source at the speed of light [6]. These cosmic ripples would move through space and time, bringing with them clues to the nature of gravity and information about their origins [26].

Published by Springer Nature Switzerland AG 2023
I. Maglogiannis et al. (Eds.): AIAI 2023, IFIP AICT 675, pp. 3–14, 2023.
https://doi.org/10.1007/978-3-031-34111-3_1

In 2015, a signal produced by the merger of two black holes, was detected by the Laser-Interferometer-Gravitational-wave-Observatory (LIGO) gravitational wave detectors in Livingston Louisiana, and Hanford Washington, which was the GWs' initial direct observation [13]. This type of detected GWs are produced by orbiting pairs of massive and dense/compact objects such as white dwarf stars, black holes, and neutron stars. Neutron stars are extremely dense objects created by collapsed stars, which run out all of their energy [1,2]. Due to the compact-binary-spinning source mechanism of this type of waves, they took the name: "*compact Binary inspiral Gravitational Waves (B-GWs)*". Furthermore, it is worth mentioning that, depending on the spinning pair's object type, the B-GWs are separated into the following three sub-categories: binary neutron star, binary black hole, neutron star-black hole binary [4,8].

However, scientists have predicted the existence of a new type of GWs called: *Continuous Gravitational Waves (C-GWs)*, which are created by the rotation of single non-perfect neutron stars spheres [3]. Unlike the complicated burst of B-GW, C-GWs are elegant, well-defined, and almost constant being able to provide much more information about universe wonders, like neutron stars. Via the detection of C-GWs we will get a better knowledge of stellar evolution and populations as well as the internal structure and evolutionary history of these exceptional and yet intriguing objects, which will offer insights into the invisible huge population of neutron stars that inhabits our Galaxy [3,24].

Unfortunately, despite all of this progress, since 2015 all of the objects LIGO has detected so far, fall only into the B-GWs category, while the direct detection of real C-GWs still remains an open problem. In contrast to the common detected B-GWs, C-GWs are much weaker, which makes them much harder to be detected. Therefore, we aim to propose a novel Deep-Learning-based methodology, being sensitive enough for detecting C-GWs.

Deep learning (DL) [22] is a subset of machine learning that utilizes neural networks with multiple layers to learn patterns and features from data. It has been particularly effective in tasks such as image and speech recognition, natural language processing, and decision making. Convolutional Neural Networks (CNNs) [10,30] are a type of DL algorithm, which are particularly well-suited for image and video processing, which were applied in a wide range of applications [14,15,18]. This type of models work by repeatedly applying a set of filters to the input data, which allows them to learn spatial hierarchies of features.

In this work, we propose a Deep-Learning methodology for detecting and visualizing C-GWs utilizing a dataset based on the LIGO laboratory. This dataset has a time-frequency form constituted of a set of Short-time Fourier Transforms (SFTs) with respect to the GPS time stamps for each interferometer (LIGO Hanford and LIGO Livingston). Each data sample contains either real or simulated noise and possibly a simulated C-GW signal, while the task is to identify when a C-GW signal is present in the data. More specifically, the main objective of our proposed methodology is to create a more robust and clear representation form removing noise, by incorporating SFT pre-processing techniques, comparing to the state-of-the-art end-to-end deep-learning baseline

approach (initial representation form of LIGO laboratory which is fed into a CNN model). The proposed transformation methodology considerably outperformed the baseline approach, for every applied experimental configuration (e.g., CNN model, input-shape, and augmentation choices) revealing the efficiency of the proposed approach.

The main contributions of this work are summarized as follows: We propose a novel pre-processing and deep-learning-based methodology for detecting and visualizing C-GWs (C-GWs are much harder to detect comparing to B-GWs), managing to achieve high accuracy comparing to the baseline approaches. The proposed method, managed to achieve a high overall performance proving to be a promising supporting tool to Astronomy and Physics Scientists for detecting possible C-GWs signals. Also, the incorporation of SpecAugm [19] methodology, drastically improved the results for every utilized model in every configuration. Finally, this work can potentially help scientists detect the new type of GWs called C-GWs, while further studies of these waves may enable scientists to learn about the structure of the most extreme stars in our universe.

To the best of our knowledge there are not any noticeable Machine-Learning-based approaches for automatic detection of Continuous-Gravitational-Waves (C-GWs), although there are plenty of research works on detection of compact Binary inspiral Gravitational Waves (B-GWs) [27,31]. Due to the complicated SFT spectrogram form of LIGO provided data, the high difficulty detection level of C-GWs, and the totally different nature and shape-form between the B-GWs and the C-GWs [3,24], it is not possible and reasonable to utilize as baseline state-of-the-art approaches the ones proposed for B-GWs detection problem.

Thus, specifically for the C-GW problem, it is reasonable to consider as state-of-the-art baseline approach, an end-to-end deep-learning-based approach utilizing the initial SFT representation form of the data provided by LIGO. In this baseline approach, the multi-channel spectrogram-based data of LIGO are fed into a multi-channel pre-trained CNN model, in order to perform the final classification. Instead, in our proposed approach, we apply SFT pre-processing and transformation techniques in order to reduce the initial high dimension, remove noise, and create a more robust representation for feeding a pre-trained CNN model in order to perform the final classification task.

2 Methodology

In this section, we describe in detail the data acquisition procedure and our proposed DL methodology for detecting possible signals of C-GW.

2.1 LIGO Interferometers

LIGO [5] is a marvel of meticulous engineering and the biggest gravitational wave observatory in the world. LIGO, consists of two enormous laser interferometers separated by 3000 km km, uses the physical characteristics of light and space itself to detect and comprehend the origins of gravitational waves. In brief,

LIGO has two gravitational-wave interferometers: LIGO Hanford (H) and LIGO Livingston (L). Each of them has two 4 km long arms arranged in the shape of an "L", acting as antennae to detect gravitational waves.

The basic operation principle in which LIGO detects GWs is briefly described as follows: Space itself is stretched by gravitational waves in one direction, while it is also compressed in the opposite direction [5]. As long as a wave is passing, the one arm of the LIGO interferometer is getting longer while the other gets shorter. In this way, LIGO is able to detect a possible GW signal. Similarly, to a human ear, which is able to detect vibrations in a medium like air or water, LIGO acts as an antenna able to detect vibrations in the "medium" of space-time.

2.2 Description of Case-Study Dataset Used for Detecting C-GWs

The frequency and amplitude of a C-GW signal from a rotating neutron star will be almost precisely constant [3]. However, over a long period of time, since the neutron star loses energy as it emits gravitational and electromagnetic waves, which causes it to rotate more slowly, the frequency of the signal gradually changes. With regard to the neutron star, the detector on Earth is moving. This alters the gravitational wave frequency that the detector picks up. Monitoring all potential frequency changes can be very computationally challenging. For this reason, Short-time Fourier Transforms (SFTs) [7] are used for quantifying the change of a non-stationary signal's frequency and phase content over time.

The utilized dataset in this research is based on the LIGO laboratory, which contains time-frequency data from two gravitational-wave interferometers: LIGO Hanford (H) and LIGO Livingston (L). Each data sample contains either real or simulated noise and possibly a simulated C-GW signal. The task is to identify when a signal is present in the data.

More specifically, each sample is comprised of a set of Short-time Fourier Transforms (SFTs) and corresponding GPS time stamps for each interferometer H and L. The SFTs are not always contiguous in time since the interferometers are not continuously online. Each sample can be represented as a spectrogram of the Real and Imaginary part of the complex form of the furrier transform corresponding to each interferometer H and L. Therefore, each sample/instance has the following initial spectrogram representation input-shape format:

$$N_{\text{inter}} \times N_{\text{complex}} \times Freq \times Time \tag{1}$$

where $N_{\text{inter}} = 2$ represents the number of interferometers, $N_{\text{complex}} = 2$ represents the number of complex parts (real and imaginary), $Freq = 360$ represents the signal's frequency and $Time$ is time in GPS timestamp.

2.3 State-of-the-Art Baseline Approach

Figure 1 presents a high-level presentation of the "*baseline approach*" (a 4 channel-CNN based on the Initial SFT spectrogram representation form of LIGO laboratory).

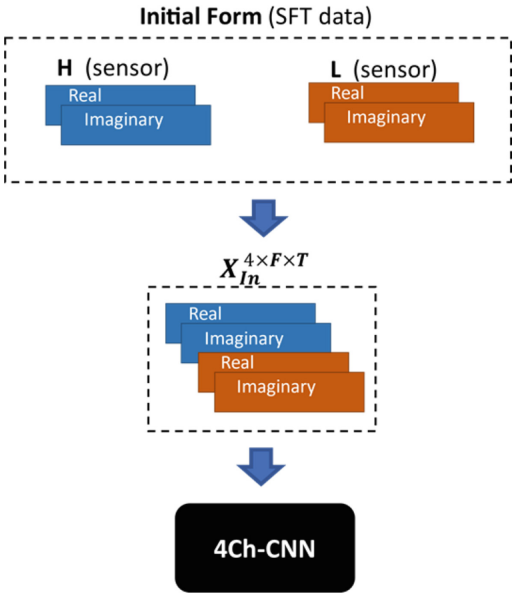

Fig. 1. Schematic presentation of the state-of-the-art end-to-end deep-learning baseline approach (a 4ch-CNN fed with the initial SFT form of LIGO laboratory)

Let assume the initial input matrices $\mathbf{H}_{\mathbb{C}}^{F\times T}$ and $\mathbf{L}_{\mathbb{C}}^{F\times T}$ corresponding to the SFT amplitudes $h_{f,t} \in \mathbb{C}$ and $l_{f,t} \in \mathbb{C}$ of the signals detected via the interferometers of LIGO Hanford (H) & LIGO Livingston (L) which are respectively defined by

$$\mathbf{H}_{\mathbb{C}}^{F\times T} = \begin{bmatrix} h_{1,1} & \cdots & h_{1,t} & \cdots & h_{1,T} \\ \vdots & \ddots & \vdots & \ddots & \vdots \\ h_{f,1} & \cdots & h_{f,t} & \cdots & h_{f,T} \\ \vdots & \ddots & \vdots & \ddots & \vdots \\ h_{F,1} & \cdots & h_{F,t} & \cdots & h_{F,T} \end{bmatrix} \quad \text{and} \quad \mathbf{L}_{\mathbb{C}}^{F\times T} = \begin{bmatrix} l_{1,1} & \cdots & l_{1,t} & \cdots & l_{1,T} \\ \vdots & \ddots & \vdots & \ddots & \vdots \\ l_{f,1} & \cdots & l_{f,t} & \cdots & l_{f,T} \\ \vdots & \ddots & \vdots & \ddots & \vdots \\ l_{F,1} & \cdots & l_{F,t} & \cdots & l_{F,T} \end{bmatrix} \tag{2}$$

where $f = 1, 2, \ldots, F$ corresponds to the frequency index, $t = 1, 2, \ldots, T$ to the timestamps-samples number and $\mathbb{C}$ to the complex numbers set. Each complex number is represented by a real and imaginary part; therefore, for the matrices defined in Eq. (2), we have

$$\mathbf{H}_{\mathbb{C}} = \mathbf{H}_{\mathbb{R}}^{F\times T} + i\mathbf{H}_{\mathbb{I}}^{F\times T} \quad \text{and} \quad \mathbf{L}_{\mathbb{C}} = \mathbf{L}_{\mathbb{R}}^{F\times T} + i\mathbf{L}_{\mathbb{I}}^{F\times T} \tag{3}$$

where i is the imaginary unit and $\mathbf{H}_{\mathbb{R}}, \mathbf{H}_{\mathbb{I}}, \mathbf{L}_{\mathbb{R}}, \mathbf{L}_{\mathbb{I}}$ correspond to the Real and Imaginary part of the $\mathbf{H}_{\mathbb{C}}$ and $\mathbf{L}_{\mathbb{C}}$ matrices, respectively. Thus, the input $\mathbf{X}_{In}^{4\times F\times T}$ as defined in Eq. (4), is fed into a 4-channel CNN, corresponds to the state-of-the-art end-to-end deep-learning-based baseline approach.

$$\mathbf{X}_{In}^{4\times F\times T} = (\mathbf{H}_{\mathbb{R}}, \mathbf{H}_{\mathbb{I}}, \mathbf{L}_{\mathbb{R}}, \mathbf{L}_{\mathbb{I}}) \times 1e^{22} \tag{4}$$

It is worth mentioning that the amplitude values $h_{f,t}$, $l_{f,t}$ range in $1e^{-22}$ order, since the initial signals detected are extremely weak. Feeding them in a CNN model would result in losing the numbers precision. For this reason, it is essential to multiply the input matrices with the term $1e^{22}$, as defined in Eq. (4).

2.4 Proposed Methodology

Figure 2 illustrates a schematic presentation of the "*proposed deep learning C-GW detection approach*".

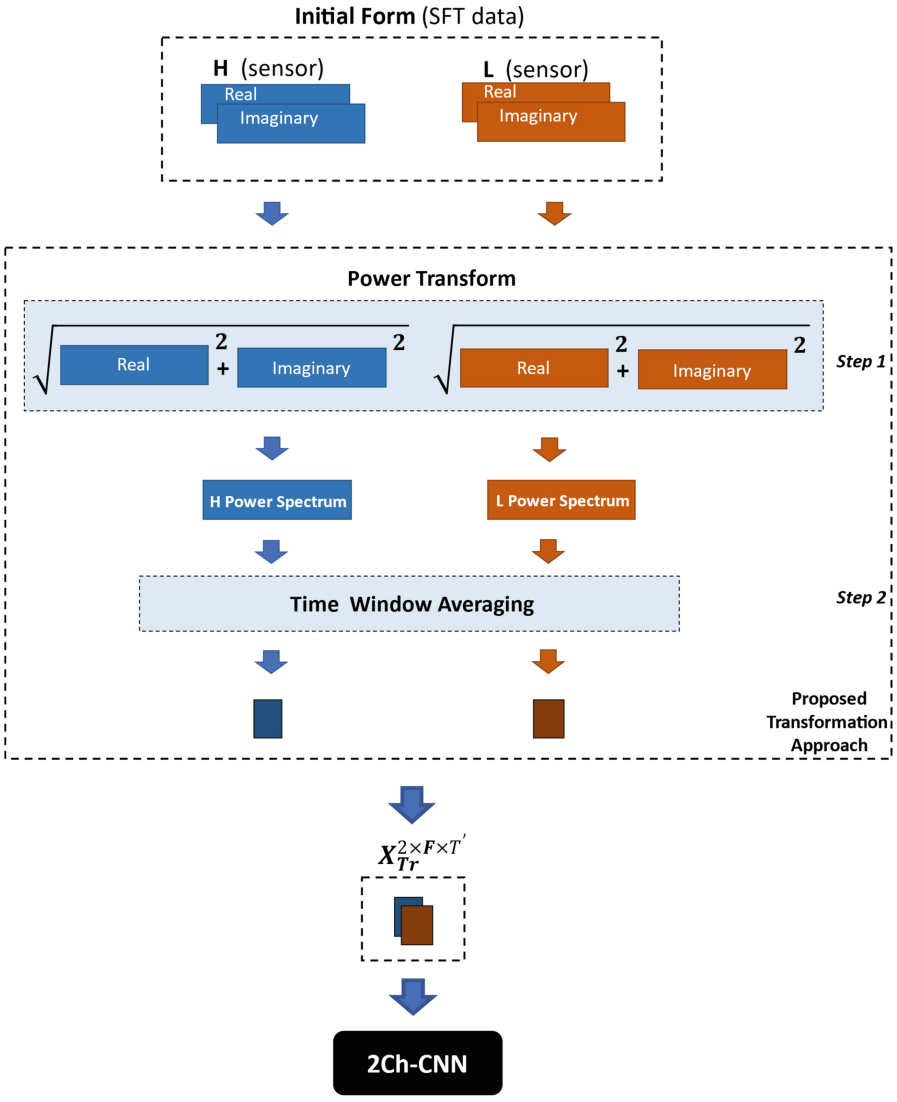

Fig. 2. Schematic presentation of the proposed DL C-GW detection approach

In order to create a robust representation and remove noise from the $\mathbf{H}_{\mathbb{C}}$ and $\mathbf{L}_{\mathbb{C}}$ spectrograms, we are able to compute their power spectrums $\mathbf{H}_P$ and $\mathbf{L}_P$ respectively (Step 1, Fig. 3), which are defined as follows:

$$\mathbf{H}_P = \begin{bmatrix} h_{1,1}^{(P)} \cdots h_{1,t}^{(P)} \cdots h_{1,T}^{(P)} \\ \vdots \ \ddots \ \vdots \ \ddots \ \vdots \\ h_{f,1}^{(P)} \cdots h_{f,t}^{(P)} \cdots h_{f,T}^{(P)} \\ \vdots \ \ddots \ \vdots \ \ddots \ \vdots \\ h_{F,1}^{(P)} \cdots h_{F,t}^{(P)} \cdots h_{F,T}^{(P)} \end{bmatrix} \quad \text{and} \quad \mathbf{L}_P = \begin{bmatrix} l_{1,1}^{(P)} \cdots l_{1,t}^{(P)} \cdots l_{1,T}^{(P)} \\ \vdots \ \ddots \ \vdots \ \ddots \ \vdots \\ l_{f,1}^{(P)} \cdots l_{f,t}^{(P)} \cdots l_{f,T}^{(P)} \\ \vdots \ \ddots \ \vdots \ \ddots \ \vdots \\ l_{F,1}^{(P)} \cdots l_{F,t}^{(P)} \cdots l_{F,T}^{(P)} \end{bmatrix} \tag{5}$$

where $h_{f,t}^{(P)} = \sqrt{(h_{f,t}^{(\mathbb{R})})^2 + (h_{f,t}^{(\mathbb{I})})^2}$ and $l_{f,t}^{(P)} = \sqrt{(l_{f,t}^{(\mathbb{R})})^2 + (l_{f,t}^{(\mathbb{I})})^2}$, while $h_{f,t}^{(\mathbb{R})}$, $h_{f,t}^{(\mathbb{I})}$, $l_{f,t}^{(\mathbb{R})}$, and $l_{f,t}^{(\mathbb{I})}$ are the amplitudes values of $\mathbf{H}_{\mathbb{R}}$, $\mathbf{H}_{\mathbb{I}}$, $\mathbf{L}_{\mathbb{R}}$ and $\mathbf{L}_{\mathbb{I}}$, respectively.

Since the data is time correlated with respect to the timestamps t, we further transform the data via a time-window-averaging approach (see Step 2 in Fig. 3), in order to further remove noise and create a compressed and even more robust final representation form, aiming to reveal possible signs of C-GWs (Fig. 4), defined as follows

$$\mathbf{H}_{PAv}^{F\times T'} = \begin{bmatrix} E\left(h_{1,1}^{(P)},\ldots,h_{1,k}^{(P)}\right) \cdots E\left(h_{1,k(j-1)}^{(P)},\ldots,h_{1,kj}^{(P)}\right) \cdots E\left(h_{1,k(T'-1)}^{(P)},\ldots,h_{1,kT'}^{(P)}\right) \\ \vdots \ \ddots \ \vdots \ \ddots \ \vdots \\ E\left(h_{f,1}^{(P)},\ldots,h_{f,k}^{(P)}\right) \cdots E\left(h_{f,k(j-1)}^{(P)},\ldots,h_{f,kj}^{(P)}\right) \cdots E\left(h_{f,k(T'-1)}^{(P)},\ldots,h_{f,kT'}^{(P)}\right) \\ \vdots \ \ddots \ \vdots \ \ddots \ \vdots \\ E\left(h_{F,1}^{(P)},\ldots,h_{F,k}^{(P)}\right) \cdots E\left(h_{F,k(j-1)}^{(P)},\ldots,h_{F,kj}^{(P)}\right) \cdots E\left(h_{F,k(T'-1)}^{(P)},\ldots,h_{F,kT'}^{(P)}\right) \end{bmatrix}$$

and

$$\mathbf{L}_{PAv}^{F\times T'} = \begin{bmatrix} E\left(l_{1,1}^{(P)},\ldots,l_{1,k}^{(P)}\right) \cdots E\left(l_{1,k(j-1)}^{(P)},\ldots,l_{1,kj}^{(P)}\right) \cdots E\left(l_{1,k(T'-1)}^{(P)},\ldots,l_{1,kT'}^{(P)}\right) \\ \vdots \ \ddots \ \vdots \ \ddots \ \vdots \\ E\left(l_{f,1}^{(P)},\ldots,l_{f,k}^{(P)}\right) \cdots E\left(l_{f,k(j-1)}^{(P)},\ldots,l_{f,kj}^{(P)}\right) \cdots E\left(l_{f,k(T'-1)}^{(P)},\ldots,l_{f,kT'}^{(P)}\right) \\ \vdots \ \ddots \ \vdots \ \ddots \ \vdots \\ E\left(l_{F,1}^{(P)},\ldots,l_{F,k}^{(P)}\right) \cdots E\left(l_{F,k(j-1)}^{(P)},\ldots,l_{F,kj}^{(P)}\right) \cdots E\left(l_{F,k(T'-1)}^{(P)},\ldots,l_{F,kT'}^{(P)}\right) \end{bmatrix}$$

where $k = \frac{T}{T'}$ is the averaging window size, $T' < T$, $k \in \mathbb{N}$ the new total timestamps of the compressed power spectrograms, and $E(\cdot)$ is the Expected value function (also called Average or Mean).

Thus, the input $\mathbf{X}_{Tr}^{2\times F\times T'}$ of the 2Ch-CNN which corresponds to the Proposed Approach is defined as:

$$\mathbf{X}_{Tr}^{2\times F\times T'} = (\mathbf{H}_{PAv}^{F\times T'}, \mathbf{L}_{PAv}^{F\times T'}) \times 1e^{22}.$$

Figure 3(a) presents an instance labeled as "C-GW" based on its initial SFT spectrogram representation form of LIGO laboratory. However, due to noise is almost impossible to identify signs of waves in this form making it appear as pure noise signal. Instead, based on the proposed transformed representation form (Fig. 3(b)), clearly signs of a C-GW are visualized[1].

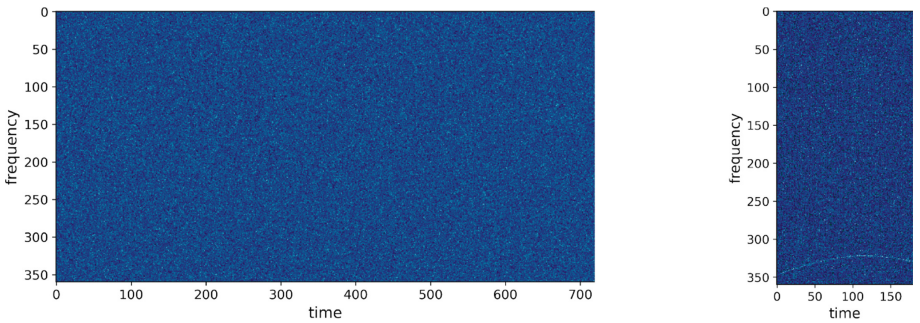

Fig. 3. Presentation of a "C-GW" instance based on (a) its initial SFT form of LIGO laboratory (a), compared to (b) its proposed transformed representation form

3 Experimental Results

In this section, we analyze and present our experimental setup, comparing the Proposed Approach, with the state-of-the-art end-to-end deep-learning approach (initial representation form of LIGO laboratory which feds a 4-channel CNN model), utilizing various CNN baselines, for different input shapes, using also sophisticated augmentation approach[2].

It is worth mentioning that the selection of the utilized CNN baselines in our experiments was based on those which managed to bring the best overall results.

Inception-v4 [28] is a deep convolutional neural network architecture for object recognition and image classification tasks being an extension of the Inception architecture. The key innovation in Inception-v4 is the use of residual connections, which have been shown to improve the performance of deep neural networks. ResNeSt [32] is a deep convolutional neural network architecture for image classification and object recognition tasks. The key innovation in ResNeSt is the use of split attention mechanism, which allows the network to attend to both global and local features simultaneously. DenseNet [11] is a deep convolutional neural network architecture for image classification and object recognition tasks. The key innovation in DenseNet is the use of dense connections, which

[1] For visualization purposes, we averaged the multi channels spectrograms to 1-channel.

[2] The datasets used in our research, can be found in https://www.kaggle.com/datasets/emmanuelpintelas/gw-datasets.

connect each layer to every other layer in a feed-forward fashion. Efficientnet-b8 [12] is a deep convolutional neural network architecture for image classification and object recognition tasks. The key innovation in EfficientNet is the use of compound scaling, which adjusts the depth, width, and resolution of the network to improve its performance.

In order to guarantee the reliability of the final experimental performance results, we performed a 5-fold-cross-validation averaging strategy for every utilized experimental configuration (CNN model, input-shape and augm. selection). The evaluation procedure was performed based on the following performance metrics: Accuracy (Acc), F_1-score (F_1), Sensitivity (Sen), Specificity (Spe), and the Area Under the Curve (AUC) [16,23].

It is worth mentioning that the initial frequency and time dimensions of every spectrogram instance 360 Hz and 4320 timestamps, respectively, which implies that for the baseline approach the input's data shape was $4 \times 360 \times 4320$. However, each utilized pre-trained model reported unsatisfactory performance. Therefore, we resized the input data to $4 \times 360 \times 720$ using bilinear interpolation, which reported the best performance. Additionally, for the proposed approach, we investigated its performance using various values for the parameter k, i.e. $2, 4, 6, 8, 12$ and 24). In our experiments, we selected $k = 6$ and $k = 24$, which implies that the input's data shapes for the proposed CNN model were $2 \times 360 \times 720$ and $2 \times 360 \times 180$, respectively.

We have also utilized the SpecAugmen [19] data augmentation method (this augmentation method was initially proposed and applied on automatic Speech Recognition), in order to prevent overfitting and increase the diversity of our training data, which managed to considerably improve the performance results.

Tables 1 and 2 summarize our experimental results. The proposed transformation methodology considerably outperformed the baseline end-to-end CNN approach (initial representation form of LIGO laboratory feeding a 4-channel CNN model), for every applied experimental configuration (e.g., CNN model, input-shape and augm. choices). The proposed method, managed to achieve a high overall performance proving to be a promising supporting tool to Astronomy and Physics Scientists for detecting possible C-GWs signals.

The incorporation of SpecAugm methodology, drastically improved the results for every utilized model in all input-shape configurations. The best results in overall were achieved for the lowest time compression size applied, while as the compression size was increased, the results significantly decreased.

Furthermore, regarding our experimental findings, it is worth mentioning that the best results in overall were achieved for the lowest time compression size applied, while as the compression size was increased, the results significantly decreased. This was probably due to the fact that on high dimensions, the input has more noise leading to model overfitting, while the C-GWs signal appear much weaker and unclear. In contrast on low sizes, the input becomes more robust enabling the C-GW signal to be much stronger and apparent assisting the CNN model to easily identify and reveal it.

Table 1. Experimental results based on the initial representation form of LIGO laboratory (baseline approach)

Augm.	CNN baseline	Input size	Acc	F_1	Sen	Spe	AUC
None	Inception-v4	$4 \times 360 \times 720$	66.5%	0.795	0.034	0.979	0.567
	ResNeSt		66.7%	0.778	0.0	1.0	0.573
	DenseNet		65.9%	0.799	0.011	0.995	0.543
	Efficientnet-b8		61.5%	0.732	0.208	0.827	0.556
SpecAugm	Inception-v4	$4 \times 360 \times 720$	66.2%	0.680	0.0	1.0	0.563
	ResNeSt		54.0%	0.551	0.534	0.533	0.547
	DenseNet		66.7%	0.789	0.0	1.0	0.564
	Efficientnet-b8		57.7%	0.659	0.335	0.697	0.571

Table 2. Experimental results based on the initial representation form of LIGO laboratory (proposed approach)

Augm.	CNN baseline	Input size	Acc	F_1	Sen	Spe	AUC
None	Inception-v4	$2 \times 360 \times 720$	66.7%	0.800	0.0	1.0	0.599
		$2 \times 360 \times 180$	65.5%	0.712	0.426	0.752	0.724
	ResNeSt	$2 \times 360 \times 720$	66.3%	0.792	0.005	0.992	0.612
		$2 \times 360 \times 180$	67.0%	0.750	0.394	0.791	0.697
	DenseNet	$2 \times 360 \times 720$	66.2%	0.791	0.070	0.958	0.622
		$2 \times 360 \times 180$	68.7%	0.757	0.553	0.753	0.762
	Efficientnet-b8	$2 \times 360 \times 720$	64.5%	0.758	0.254	0.851	0.624
		$2 \times 360 \times 180$	66.5%	0.763	0.381	0.823	0.750
SpecAugm	Inception-v4	$2 \times 360 \times 720$	62.2%	0.694	0.487	0.700	0.684
		$2 \times 360 \times 180$	66.5%	0.757	0.378	0.818	0.751
	ResNeSt	$2 \times 360 \times 720$	60.8%	0.640	0.757	0.545	0.709
		$2 \times 360 \times 180$	66.8%	0.754	0.458	0.777	0.752
	DenseNet	$2 \times 360 \times 720$	64.0%	0.744	0.319	0.815	0.671
		$2 \times 360 \times 180$	69.6%	0.775	0.511	0.793	0.774
	Efficientnet-b8	$2 \times 360 \times 720$	66.5%	0.798	0.0	0.997	0.661
		$2 \times 360 \times 180$	70.3%	0.748	0.782	0.667	0.796

4 Conclusions

In this work, we proposed a novel pre-processing and deep-learning-based methodology for detecting and visualizing C-GWs utilizing a dataset based on the LIGO laboratory as case-study scenario. This dataset has time-frequency form based on two gravitational-wave interferometers: LIGO Hanford and LIGO

Livingston. Each data sample contained either real or simulated noise and possibly a simulated C-GW signal. In brief, the task was to identify when a C-GW signal is present in the data.

Our proposed methodology aimed to create a more robust and clear representation form in order to feed a CNN model. Based on extensive experimental simulations, our approach significantly outperformed the state-of-the-art end-to-end deep-learning approach, for every applied experimental configuration, revealing the efficiency of the proposed methodology and proving to be a promising supporting tool to Astrophysical scientists for detecting possible C-GWs signals.

The con of this works lies on the fact that no time-series-based approached were investigated, since the initial type of data are time-correlated. Thus, in our future research, we intent to further improve our model's detection sensitivity by incorporating statistical analysis and time-series enhancing approaches [14,17]. Finally, we also intend to improve our work by adding the Explainability/Interpretability property [20,21,25] to our detection approach, which is obviously of crucial significance in Astrophysical sciences for unveiling and explaining the mysteries of Universe.

References

1. Abbott, B.P., et al.: GW170817: observation of gravitational waves from a binary neutron star inspiral. Phys. Rev. Letters **119**(16), 161101 (2017)
2. Abbott, B.P., et al.: Observation of gravitational waves from a binary black hole merger. Phys. Rev. Lett. **116**(6), 061102 (2016)
3. Abbott, B.P., Abbott, R., Abbott, T., Abraham, S., Acernese, F., Ackley, K., et al.: All-sky search for continuous gravitational waves from isolated neutron stars using advanced LIGO O2 data. Phys. Rev. D **100**(2), 102008 (2019)
4. Abbott, B.P., et al.: Exploring the sensitivity of next generation gravitational wave detectors. Classical and Quantum Gravity **34**(4), 044001 (2017)
5. Abbott, B., et al.: LIGO: the laser interferometer gravitational-wave observatory. Reports Progress Phys. **72**(7), 076901 (2009)
6. Abbott, R., et al.: Searches for gravitational waves from known pulsars at two harmonics in the second and third LIGO-Virgo observing runs. Astrophys J **935**(1), 1 (2022)
7. Byrne, C.L.: Signal Processing: a mathematical approach. CRC Press (2014)
8. Caprini, C., Figueroa, D.G.: Cosmological backgrounds of gravitational waves. Classical Quant. Gravity **35**(16), 163001 (2018)
9. George, D., Huerta, E.A.: Deep learning for real-time gravitational wave detection and parameter estimation: results with advanced LIGO data. Phys. Lett. B **778**, 64–70 (2018)
10. He, K., Zhang, X., Ren, S., Sun, J.: Deep residual learning for image recognition. In: Proceedings of the IEEE Conference on Computer Vision and Pattern Recognition, pp. 770–778 (2016)
11. Huang, G., Liu, Z., Van Der Maaten, L., Weinberger, K.Q.: Densely connected convolutional networks. In: Proceedings of the IEEE Conference on Computer Vision and Pattern Recognition, pp. 4700–4708 (2017)
12. Koonce, B., Koonce, B.: Efficientnet. Convolutional Neural Networks with Swift for Tensorflow: Image Recognition and Dataset Categorization, pp. 109–123 (2021)

13. Królak, A., Patil, M.: The first detection of gravitational waves. Universe **3**(3), 59 (2017)
14. Livieris, I.E., Pintelas, E., Kiriakidou, N., Stavroyiannis, S.: An advanced deep learning model for short-term forecasting us natural gas price and movement. In: Artificial Intelligence Applications and Innovations, pp. 165–176. Springer (2020)
15. Livieris, I.E., Pintelas, E., Pintelas, P.: A CNN-LSTM model for gold price time-series forecasting. Neural Comput. Appl. **32**, 17351–17360 (2020)
16. Livieris, I.E., Pintelas, P.: An adaptive nonmonotone active set-weight constrained-neural network training algorithm. Neurocomputing **360**, 294–303 (2019)
17. Livieris, I.E., Stavroyiannis, S., Pintelas, E., Pintelas, P.: A novel validation framework to enhance deep learning models in time-series forecasting. Neural Comput. Appl. **32**(23), 17149–17167 (2020). https://doi.org/10.1007/s00521-020-05169-y
18. Lu, L., Zheng, Y., Carneiro, G., Yang, L.: Deep learning and convolutional neural networks for medical image computing. Adv. Comput. Vis. Pattern Recognit. **10**, 978–3 (2017)
19. Park, D.S., et al.: Specaugment: A simple data augmentation method for automatic speech recognition. arXiv preprint arXiv:1904.08779 (2019)
20. Pintelas, E., Liaskos, M., Livieris, I.E., Kotsiantis, S., Pintelas, P.: A novel explainable image classification framework: Case study on skin cancer and plant disease prediction. Neural Comput. Appl. **33**(22), 15171–15189 (2021)
21. Pintelas, E., Livieris, I.E., Pintelas, P.: A grey-box ensemble model exploiting black-box accuracy and white-box intrinsic interpretability. Algorithms **13**(1), 17 (2020)
22. Purwins, H., Li, B., Virtanen, T., Schlüter, J., Chang, S.Y., Sainath, T.: Deep learning for audio signal processing. IEEE J. Selected Topics Signal Process. **13**(2), 206–219 (2019)
23. Raschka, S.: An overview of general performance metrics of binary classifier systems. arXiv preprint arXiv:1410.5330 (2014)
24. Riles, K.: Recent searches for continuous gravitational waves. Mod. Phys. Lett. A **32**(39), 1730035 (2017)
25. Roscher, R., Bohn, B., Duarte, M.F., Garcke, J.: Explainable machine learning for scientific insights and discoveries. IEEE Access **8**, 42200–42216 (2020)
26. Rothman, T.: The secret history of gravitational waves: contrary to popular belief, einstein was not the first to conceive of gravitational waves-but he was, eventually, the first to get the concept right. Am. Sci. **106**(2), 96–104 (2018)
27. Schäfer, M.B., Ohme, F., Nitz, A.H.: Detection of gravitational-wave signals from binary neutron star mergers using machine learning. Physical Review D **102**(6), 063015 (2020)
28. Szegedy, C., Ioffe, S., Vanhoucke, V., Alemi, A.: Inception-v4, inception-resnet and the impact of residual connections on learning. In: Proceedings of the AAAI Conference on Artificial Intelligence, vol. 31 (2017)
29. Szegedy, C., Liu, W., Jia, Y., Sermanet, P., Reed, S., Anguelov, D., Erhan, D., Vanhoucke, V., Rabinovich, A.: Going deeper with convolutions. In: Proceedings of the IEEE Conference on Computer Vision and Pattern Recognition, pp. 1–9 (2015)
30. Véstias, M.P.: Convolutional neural network. In: Encyclopedia of Information Science and Technology, Fifth Edition, pp. 12–26. IGI Global (2021)
31. Wei, W., Huerta, E.: Deep learning for gravitational wave forecasting of neutron star mergers. Phys. Lett. B **816**, 136185 (2021)
32. Zhang, H., et al.: Resnest: Split-attention networks. In: IEEE/CVF Conference on Computer Vision and Pattern Recognition, pp. 2736–2746 (2022)